JOURNAL OF SPACECRAFT AND ROCKETS
Vol. 41, No. 6, November–December 2004

Hybrid Precise Orbit Determination Strategy by Global Positioning System Tracking

Seungwoo Lee*
Korea Advanced Institute of Science and Technology, Daejeon 305-701, Republic of Korea
and
Bob E. Schutz† and P. A. M. Abusali‡
University of Texas at Austin, Austin, Texas 78712

A numerical simulation study was performed to investigate the effects of process noise modeling on state estimates of a low-Earth-orbiting satellite in the global positioning system-based hybrid precise orbit determination (POD) strategy. The use of simulated data enabled the creation of the simulated data with three different correlation types of the unknown forces. The simulation results indicate that the use of a periodic random process noise model in hybrid POD strategy provides better performance than the use of a first-order Gauss–Markov random process. The hybrid POD results obtained when the real tracking data from CHAMP (Challenging Minisatellite Payload) were processed showed improved performance of periodic random process over a first-order Gauss–Markov random process. As a relative measure of orbit accuracy, the hybrid orbit solution was compared against a reference orbit solution, and the results indicate that the radial orbit accuracy of the hybrid solution is within 6 cm, in an rms sense. As an absolute measure of orbit accuracy, satellite laser range residuals were analyzed, and the results indicate that the radial orbit accuracy of the hybrid solution is at the level of 3-cm rms for the CHAMP orbit with 460-km altitude.

Nomenclature

a_e = equatorial radius of the Earth
E = expectation operator
f = flattening factor of the Earth
P = solar radiation pressure
p = correlated process noise
Q = noise covariance matrix
R = square root information matrix
u = Gaussian white noise
β = correlation time constant
σ = steady-state uncertainty or standard deviation
Ψ = state transition matrix
ω = frequency of process noise

Subscripts

j = jth stage
N = cross-track direction
R = radial direction
T = along-track direction

Introduction

PRECISE orbit determination (POD) of satellites has become a fundamental problem in modern space operations and satellite applications, such as geodesy, navigation, communications, and many other areas. The quality of the data products obtained with satellite altimetry, for example, strongly depends on the radial accuracy of the satellite orbit. Because an accurate force model is a crucial factor to the traditional dynamic POD, extensive research has been conducted to improve and standardize those models, in parallel with efforts on the strategies for POD.

As a result of these efforts, a comprehensive set of force models has been developed during the past decades, including refined models for Earth gravity. However, the operational strategy for POD has been predominantly based on describing the satellite dynamics, typically implemented with batch filter. For example, the Geodynamics Analysis Software Package (GEODYN) at the NASA Goddard Space Flight Center and the Multi-Satellite Orbit Determination Program (MSODP) and the University of Texas Orbit Processor Incorporating Statistical Analysis (UTOPIA) at the University of Texas Center for Space Research (CSR) are all based on the epoch state batch filter, according to the dynamic strategy. This is in part because the dynamic strategy was suited for the gravity model improvement, which is one of the important applications of POD. Moreover, the data provided by the traditional ground-based tracking systems have been noisy and sparse, which can limit the accuracy of nondynamic strategies. Innovation in tracking systems is exemplified by the global positioning system (GPS). Compared with the ground-based tracking systems such as satellite laser ranging (SLR) and Doppler orbitography and radio positioning integrated by satellite (DORIS), GPS has the advantage of providing three-dimensional, global, and continuous tracking data with high precision, which enables the space-based POD.

An outstanding illustration of the GPS-based POD is with the TOPEX (Topography Experiment)/Poseidon (T/P) altimetric satellite mission[1] that was jointly conducted by NASA and the French Centre National d'Etudes Spatiales. Radial accuracy of the T/P orbit has been consistently demonstrated to be about 2–3 cm rms (Refs. 2–4). This was unprecedented, given that the prelaunch mission requirement for the radial accuracy was stated to be 13-cm rms or better. This accuracy was achieved partly because of the relatively high altitude of the T/P, which resulted in smaller error contributions from the geopotential and atmospheric drag, but also partly because of the refinement of the force models, particularly the gravity model. The T/P experience has shown that accuracy of the T/P orbit computed using the reduced-dynamic POD strategy,[3] coupled with GPS tracking data, was equal to or slightly better than that of orbits computed using dynamic strategy and SLR/DORIS data.[5] The reduced-dynamic POD strategy, implemented in the GIPSY OASIS II software package at NASA Jet Propulsion Laboratory (JPL),

Received 13 March 2003; revision received 13 August 2003; accepted for publication 14 October 2003.

*Research Associate, Department of Mechanical Engineering, 373-1, Guseong-Dong, Yuseong-Gu.
†Professor, Department of Aerospace Engineering and Engineering Mechanics. Member AIAA.
‡Research Scientist, Center for Space Research.

California Institute of Technology, utilizes the square root information filter and square root information smoother with process noise compensation.[6] This strategy is also referred to as a hybrid strategy because optimal relative weight to the dynamic information and kinematic information is sought by the adjustment of process noise, which is modeled as a first-order Gauss–Markov random process. Decreasing the steady-state uncertainty of the process noise results in migration of the solution orbit toward the dynamic orbit, whereas increasing the steady-state uncertainty renders the solution orbit to migrate toward the kinematic solution.

The objective of this study is to develop a hybrid GPS-based POD solution for satellites in low altitude orbits on a personal computer platform. To carry out the proposed study, efforts were made to develop a hybrid POD software system that utilizes the GPS double-differenced high–low (DDHL) phase range measurements.[7] As a result, the hybrid POD software package, GV3, was coded and tested. The hybrid strategy implemented in GV3 is similar to the reduced dynamic strategy of JPL's GIPSY OASIS II in the sense that a dynamic reference orbit is computed before the final filtering/smoothing and the effects of unknown forces are accommodated by use of process noise. Differences that could be found between the two software systems are that in GIPSY OASIS II, a first-order Gauss–Markov random process is employed as process noise, and undifferenced GPS measurements are used, whereas periodic random process and double-differenced GPS measurements are utilized in GV3.

Emphasis in this study is placed on the treatment of the unmodeled or mismodeled forces. To illustrate the effect of different process noise models, data with different characteristics were simulated and processed by the GV3.

However, the models used in the simulations are only approximations and can never perfectly model the real world. Accordingly, real tracking data of the low-Earth-orbiting (LEO) satellite CHAMP (Challenging Minisatellite Payload) was processed with the hybrid strategy. CHAMP occupies an orbit that is three times lower than that of T/P and, consequently, is subjected to more perturbations due to gravity and atmospheric drag errors. After the CHAMP tracking data were processed, the relative performance of two process noise models was evaluated. By use of the various measures such as orbit comparison and SLR residual analysis, the radial orbit accuracy of the hybrid solution was also assessed. Such assessment of GPS-based POD on the CHAMP orbit will be a good preliminary case for the future POD of low-altitude satellites.

Numerical Simulations

In the hybrid POD strategy, the state and covariance of satellites are influenced by the process noise, and the results of research shows the importance of proper modeling of process noise. A set of simulated data was generated with various types of forces, and the performance of a first-order Gauss–Markov process and periodic random process are assessed, respectively, and compared with each other.

Unknown Force Model

For a hybrid POD filter to accommodate unmodeled dynamics efficiently, it is important to select a suitable random process model for the unknown force. A useful model of the process noise is the first-order Gauss–Markov process. The differential equation for this process is written as

$$\dot{p} = -\beta p + u \tag{1}$$

The discrete version of Eq. (1) is described by

$$p_{j+1} = \exp[-\beta(t_{j+1} - t_j)]p_j + u_j \tag{2}$$

Q and Ψ of the process are assumed to be diagonal, so that the unmodeled accelerations are uncorrelated with each other.

In general, the choice of a model for the process noise is based on knowledge of underlying physical mechanism, but also on the degree to which model fits the data. For the orbit determination problem, unmodeled or mismodeled accelerations tend to be of periodic signature. This is partly because of the cyclic motion of the satellite. This study proposes to approximate unknown forces as a periodic random process. In this study, the adopted process noise model is assumed to be governed by the following stochastic differential equations:

$$\dot{p}_1 = p_2 + u, \qquad \dot{p}_2 = -\alpha^2 p_1 - 2\beta p_2 + (\alpha - 2\beta)u \tag{3}$$

where

$$\alpha = (\beta^2 + \omega^2)^{\frac{1}{2}}$$

An associated autocorrelation function is given by

$$\varphi_{pp}(\tau) = \sigma^2 e^{-\beta|\tau|}\cos\omega|\tau| \tag{4}$$

The discrete version of Eq. (3) can be written as

$$\begin{bmatrix} p_1 \\ p_2 \end{bmatrix}_{j+1} = \begin{bmatrix} \Psi_{11}(t_{j+1}, t_j) & \Psi_{12}(t_{j+1}, t_j) \\ \Psi_{21}(t_{j+1}, t_j) & \Psi_{22}(t_{j+1}, t_j) \end{bmatrix} \begin{bmatrix} p_1 \\ p_2 \end{bmatrix}_j + \begin{bmatrix} u_1 \\ u_2 \end{bmatrix}_j \tag{5}$$

With

$$\Delta_j = t_{j+1} - t_j$$

let

$$\Psi(t_{j+1}, t_j) = \begin{bmatrix} \Psi_{11}(t_{j+1}, t_j) & \Psi_{12}(t_{j+1}, t_j) \\ \Psi_{21}(t_{j+1}, t_j) & \Psi_{22}(t_{j+1}, t_j) \end{bmatrix} = \exp(-\beta\Delta_j)$$

$$\times \begin{bmatrix} \cos(\omega\Delta_j) + \dfrac{\beta}{\omega}\sin(\omega\Delta_j) & \dfrac{\sin(\omega\Delta_j)}{\omega} \\ -\sin(\omega\Delta_j)\left(\dfrac{\beta^2}{\omega} + \omega\right) & \cos(\omega\Delta_j) - \dfrac{\beta}{\omega}\sin(\omega\Delta_j) \end{bmatrix}$$

$$u_j = \begin{bmatrix} u_1 \\ u_2 \end{bmatrix}_j = \int_{t_j}^{t_{j+1}} \begin{bmatrix} \Psi_{11}(t_{j+1}, \tau) & \Psi_{12}(t_{j+1}, \tau) \\ \Psi_{21}(t_{j+1}, \tau) & \Psi_{22}(t_{j+1}, \tau) \end{bmatrix} \begin{bmatrix} u(\tau) \\ (\alpha - 2\beta)u(\tau) \end{bmatrix} \mathrm{d}\tau$$

Together with the governing stochastic differential equation of the process, specification of the strength of driving noise is required to characterize a random process. By the use of the expectation operator inside the integral and the use of the property of the Dirac delta function, the covariance of u_j, Q_u is computed as

$$Q_u = R^{-1}R^{-T} = E\left[u_j u_j^T\right] \tag{6}$$

In GV3, Eqs. (5) and (6) are used to implement the periodic random process model.

Case Study

The unknown force models used in the simulated study are summarized in Table 1. In case 1, the constant unmodeled force is simulated. Provided that an unmodeled mass exists near or at the center of the Earth, gravitational attraction of the mass to a satellite in a circular orbit can be reasonably approximated as a constant force in the radial direction. A constant force in the along-track direction can be an approximation of an atmospheric drag experienced by a satellite orbiting at a constant speed in a uniform density atmosphere. Also, if a satellite has an internal source of constant heat flux whose direction is always normal to orbital plane, the force due to thermal imbalance may be modeled by a constant force in the cross-track direction. In case 2, the unmodeled force model that exhibits exponentially decreasing behavior is presented. An exponentially correlated force can be utilized to model the effects of gas leak, solar wind, etc. Case 3 is a representation of the periodic unmodeled force.

Note that in cases 1–3, the magnitudes of unknown force models are made to be of the same order by scaling with a factor of $\varepsilon = 1.0 \times 10^{-6}$. In cases 1–3, no dynamic model errors other than the unknown forces were introduced in generating the simulated

data. The components of the unmodeled forces were computed according to the corresponding force model and incorporated into the integration.

For each case considered, DDHL tracking data for two orbital periods of a LEO satellite were generated with 30-s spacing. The cycle ambiguity for DDHL data was all set to zero and the signal transmission-related errors, such as ionospheric dispersion and tropospheric refraction, were neglected for the convenience of generating the simulated data. Observation noise was added to the simulated tracking data, which were the output of Gaussian white random sequence with zero mean and a specified standard deviation. The uncertainty of the observation noise generated was 0.01 m. These simulated data were processed by the GV3 without the knowledge of unmodeled forces. To assess the hybrid orbit accuracy, two different hybrid solutions were obtained with different process noise models: a first-order Gauss–Markov random process and periodic random process.

Case 1

To determine the effect of the unmodeled forces on deviation of the orbit, the truth orbit of case 1 was compared with the orbit integrated without the unmodeled forces. The position difference is shown in Fig. 1. Note that the difference is initially zero and grows with time in an unbounded manner. After completing two revolutions, the final deviations in position are approximately 200 m in the Z direction and 400 m in the X and Y directions, which implies that the specified unmodeled forces are very significant.

For a first-order Gauss–Markov process, the parameters to be specified are time constant and steady-state uncertainty. In cases 1–3, the time constant is set to 5 min and steady-state uncertainty to 1.0×10^{-7} m/s^2. For other values of the time constant, it has been reported by Muellerschoen et al.[8] that the reduced-dynamic orbit accuracy appears to be fairly insensitive to time-constant value. For the optimal steady-state uncertainty, it is empirically determined, in general, in such a way that certain performance indices, such as radial orbit overlap, are minimized. In the simulation study, however, the truth orbit is available and the orbit error can thereby be computed directly by comparing a solution orbit with the truth orbit. In this study, a steady-state uncertainty of 1.0×10^{-7} m/s^2 is used, which is selected from a one-parameter search on the optimal steady-state uncertainty by fixing the time constant. Orbit error rms obtained with different noise levels is summarized in Table 2. Note from Table 2 that any level of steady-state uncertainty in the range from 1.0×10^{-5} to 1.0×10^{-8} m/s^2 yields millimeter-level rms orbit errors in all three directions.

For a periodic random process, the time-constant and steady-state uncertainty values were the same as those used in the first-order Gauss–Markov (G–M) process. The additional parameter, namely, the frequency, was set to 1.0×10^{-5} rad/s. With such a low frequency (compared to the orbit frequency), the process would have virtually no periodic signature, and it was found that the frequency lower than 1.0×10^{-5} hardly caused any effects on the results.

The hybrid solution obtained with the first-order G–M process is plotted in Figs. 2–4. The smoothed estimates of the unknown force are shown in Fig. 2a. The associated covariance of the smoothed estimates is plotted in Fig. 3a. The time-averaged values of the

Table 2 Summary of case 1 rms orbit errors with steady-state uncertainty

Steady-state uncertainty, m/s^2	Radial rms error, m	Along-track rms error, m	Cross-track rms error, m
1.0×10^{-5}	0.0097	0.0063	0.0056
1.0×10^{-6}	0.0066	0.0038	0.0037
1.0×10^{-7}	0.0045	0.0023	0.0023
1.0×10^{-8}	0.0096	0.0045	0.0036
1.0×10^{-9}	0.2723	0.0507	0.0706

Table 1 Unknown force models used in generating simulated data and associated truth orbits

Case	$\boldsymbol{f}_{\text{unknown}} = [f_R, f_T, f_N]$
1	$f_R = 1.5\varepsilon, \quad f_T = -3.5\varepsilon, \quad f_N = 2.5\varepsilon$ where $\varepsilon = 1.0 \times 10^{-6}$ m/s^2
2	$f_R = 1.5\varepsilon[1 + \exp(-\Delta)], \quad f_T = -3.5\varepsilon[1 + \exp(-\Delta)]$ $f_N = 2.5\varepsilon[1 + \exp(-\Delta)]$ where $\varepsilon = 1.0 \times 10^{-6}$ m/s^2, $\quad \Delta = \text{mod}\,(t, 300.0)/300.0$
3	$f_R = 1.5\varepsilon[1 + \exp(-\Delta)]\sin(2\pi\varpi_1 t), \quad f_T = -3.5\varepsilon[1 + \exp(-\Delta)]\sin(2\pi\varpi_2 t)$ $f_N = 2.5\varepsilon[1 + \exp(-\Delta)]\sin(2\pi\varpi_1 t)$ where $\varepsilon = 1.0 \times 10^{-6}$ m/s^2, $\quad \Delta = \text{mod}\,(t, 300.0)/300.0$ $\omega_1 = 8.333 \times 10^{-4}, \quad \omega_2 = 1.666 \times 10^{-3}$

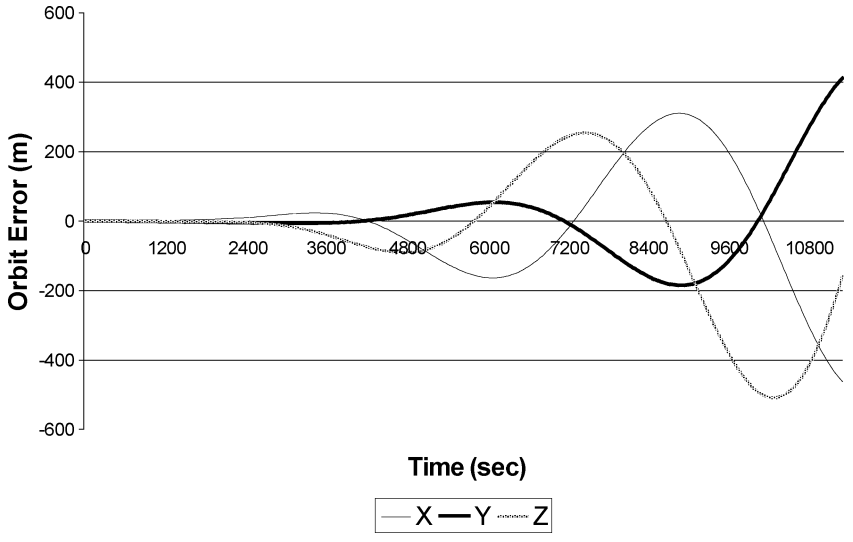

Fig. 1 Perturbation in positions due to case 1 unknown force.

Table 3 Results of unknown force estimation[a]

		GM1 process		Periodic process	
Component	True value	Estimate	Uncertainty	Estimate	Uncertainty
Radial	1.50	1.45	±0.047	1.45	±0.014
Along track	−3.50	−3.51	±0.042	−3.51	±0.011
Cross track	2.50	2.50	±0.040	2.50	±0.010

[a]Units in 1.0×10^{-6} m/s^2.

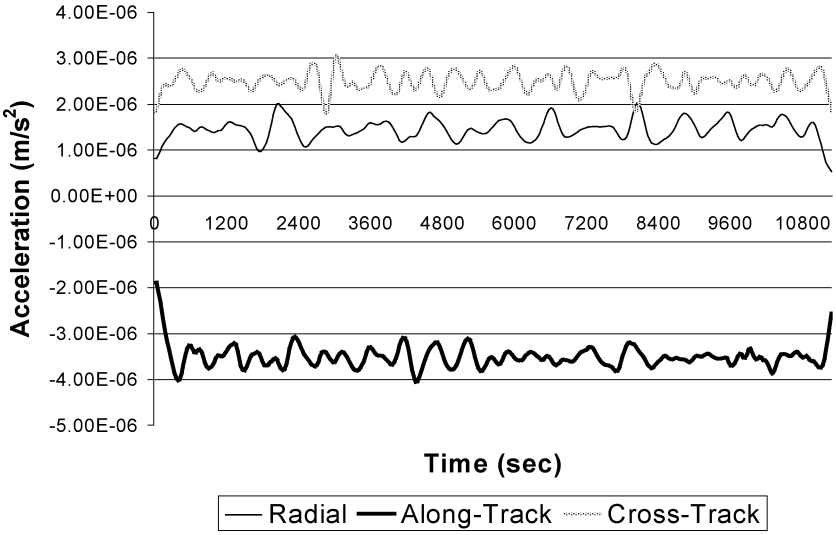

a) GM1 process

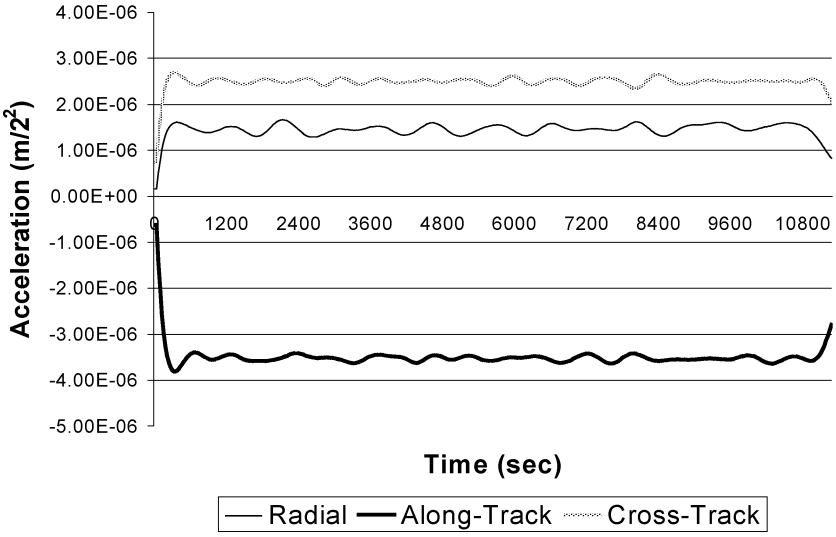

b) Periodic process

Fig. 2 Case 1 unknown force estimates.

estimate and uncertainty that are computed from the error covariance are summarized in Table 3. The radial, traverse, normal (RTN) orbit errors of hybrid solution obtained with the first order G–M process are shown in Fig. 4a. Note from Fig. 4a that the hybrid orbit solution yields good agreement with the truth orbit, and all three components of the smoothed orbit error are within the ±0.01-m region, resulting in an rms orbit error that is lower than the level of observation noise.

To illustrate the effectiveness of the hybrid strategy with a periodic random process, it is convenient to compare Figs. 2a, 3a, and 4a with results obtained from the first-order G–M process. When the estimates of unknown forces shown in Fig. 2b are compared with those shown in Fig. 2a, note that the smoothed estimate associated with the periodic process looks more consistent and less diverse than its G–M counterpart. The covariance associated with the unknown force estimates is plotted in Fig. 3b. The time-averaged values of the estimate and uncertainty obtained with the periodic process are summarized in the rightmost columns of Table 3. The uncertainty computed with the periodic process reflects the actual estimate error relatively better, compared to the covariance associated with the acceleration estimates obtained for the first-order G–M process. The RTN orbit errors obtained with the periodic process are shown in Fig. 4b. In comparison with the orbit error obtained with the first-order G–M process, the orbit error obtained with periodic process is within ±0.005 m, except for the rightmost region, resulting in slightly better rms orbit error.

Case 2

From case 1, it can be concluded that the state of the low-altitude satellite can be accurately estimated in the presence of constant unknown force according to the hybrid POD strategy, either with the

first-order G–M process or with the periodic process noise model. The experiment also shows that the rms orbit error of both solution orbits is below the uncertainty of observation noise. In contrast to the constant unknown force of case 1, the unknown force of case 2 is exponentially decreasing with time, but the magnitude of the force is about the same as that of case 1. This suggests that the magnitude of the perturbation to the orbit caused by the case 2 unknown force is similar to that of case 1. Thus, the values of the process noise model parameters, including the steady-state uncertainty, were chosen to be the same as those of case 1.

The orbit error obtained with the first-order G–M process is shown in Fig. 5a. All three components of the orbit error are generally within the ± 0.01-m region, with the prominent peaks appearing in the final few minutes. Note that the locations of the peak error in the radial direction generally coincide with those in the along-track direction. A similar signature was observed in case 1, indicating the correlation of both directions. The mean and rms orbit errors obtained when case 2 data are processed with the first-order G–M process are shown in Table 4. Note that the mean orbit error of the cross-track direction with respect to the truth orbit is less than those of the radial and along-track directions by approximately an order of magnitude, with all three values being negative. Note again that the smoothed orbit errors are, in an rms sense, below the observation noise sigma.

Numerical results of the hybrid solution obtained with a periodic random process are plotted in Fig. 5b. In comparison with case 1, the difference of the orbit error between the first-order G–M and periodic random processes is slightly reduced. This indicates that the first-order G–M process is more effective for the exponentially correlated acceleration case than for the constant acceleration case. However, the orbit obtained with periodic process still provides slight improvement over that obtained with the first-order G–M. Note that the smoothed orbit error, in the radial component, is the greatest at the final time. The reason for this is that, at the final time, the smoothed estimate is identical with that of the filtered estimate resulting in no improvement in the estimate through smoothing. The statistical summary of the orbit error obtained with the periodic process is shown in Table 4. The smoothed mean orbit errors are of same sign, whereas the magnitude of the mean error in the cross track

Table 4 Summary of case 2 orbit errors

	Mean orbit error, m			RMS orbit error, m		
Process	*R*	*T*	*N*	*R*	*T*	*N*
GM1	−0.00165	−0.00113	−0.00049	0.00645	0.00316	0.00253
Periodic	−0.00216	−0.00100	−0.00026	0.00601	0.00258	0.00180

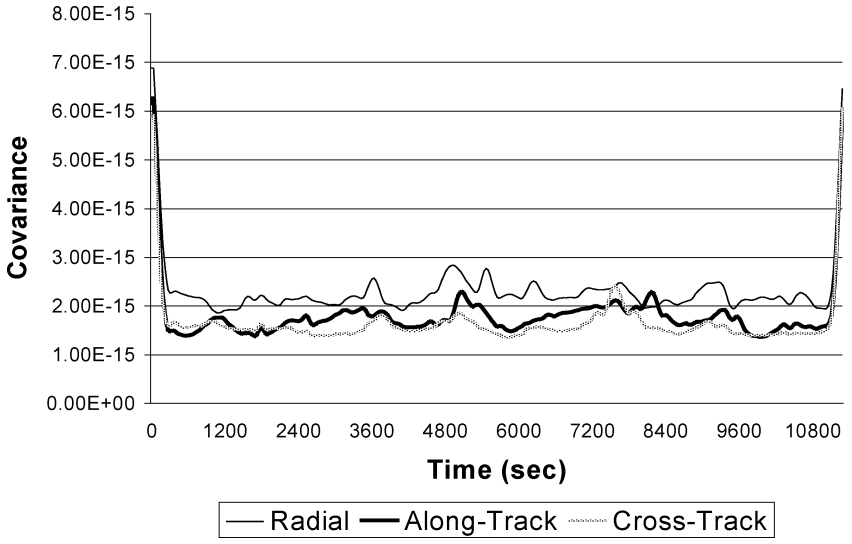

a) GM1 process

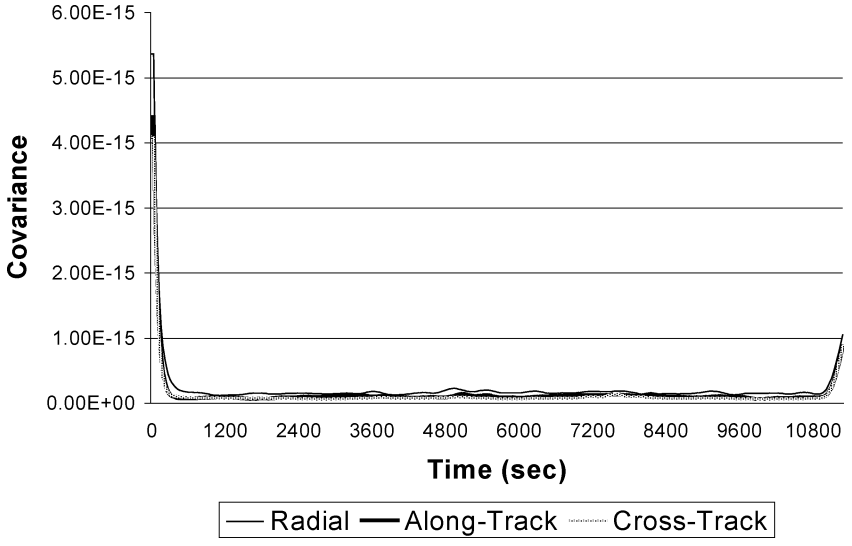

b) Periodic process

Fig. 3 Case 1 unknown force covariance.

is less than the other two components by an order of magnitude. Note that the rms orbit errors are close to each other, with periodic process-generated orbits being slightly closer to the truth, indicating that the hybrid strategy associated with the periodic process is successfully mitigating the effect of an exponentially correlated unmodeled force.

In conclusion, the hybrid strategy associated with either the first-order G–M or periodic process yields orbits statistically similar when compared with the truth orbit under the influence of the unknown force that has an exponential correlation.

Case 3

The unknown force considered in the simulation of case 3 exhibits periodic behavior. The radial and cross-track components of the unknown force have a period of 20 min, whereas the peak amplitude associated with this frequency is identical to that of case 2. The along-track component has a period of 10 min, indicating that the along-track component varies twice as rapidly as the other components. The noise parameters, such as time constant and steady-state covariance, are held fixed to the same values as in the preceding case.

Based on the unknown force model of case 3, the radial and cross-track frequencies of 5.2×10^{-3} rad/s and along-track frequency of 1.1×10^{-2} rad/s were selected, so that a known accurate measurement of the frequencies is used. It is expected that a periodic process would be more effective in case 3 because the unknown force of case 3 is periodic.

The orbit error obtained with the first-order G–M process is shown in Fig. 6a. In Fig. 6a, the periodicity of the orbit error is evident, which is clearly due to the effects of the unmodeled force. The orbit errors in all three components are generally within ± 0.02 m, with the prominent peak being about 0.055 m. The periodicity in the peak orbit error is more pronounced, particularly in the along-track component that results from the sinusoidal variation of 10-min period. The radial orbit error exhibits periodicity of 20 min, which is to be expected, and is modulated by 10-min variation of the along-track component. The mean and rms orbit errors are summarized in Table 5. Note from Table 5 that the rms orbit error obtained with the first-order G–M process is relatively noisy, particularly in the radial and along-track directions, given that in cases 1 and 2

Table 5 Summary of case 3 orbit errors

	Mean orbit error, m			RMS orbit error, m		
Process	*R*	*T*	*N*	*R*	*T*	*N*
GM1	−0.00232	−0.00349	−0.00121	0.01173	0.01414	0.00656
Periodic	−0.00061	−0.00239	−0.00086	0.00601	0.00622	0.00389

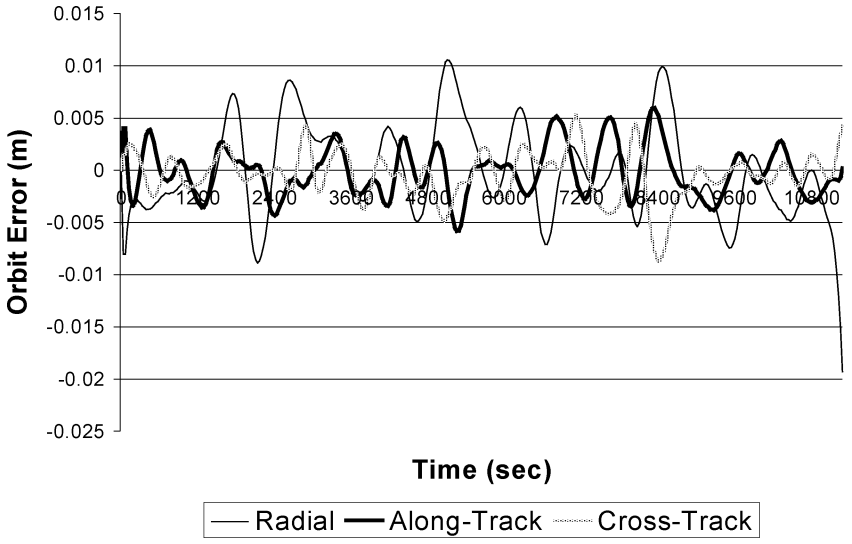

a) GM1 process

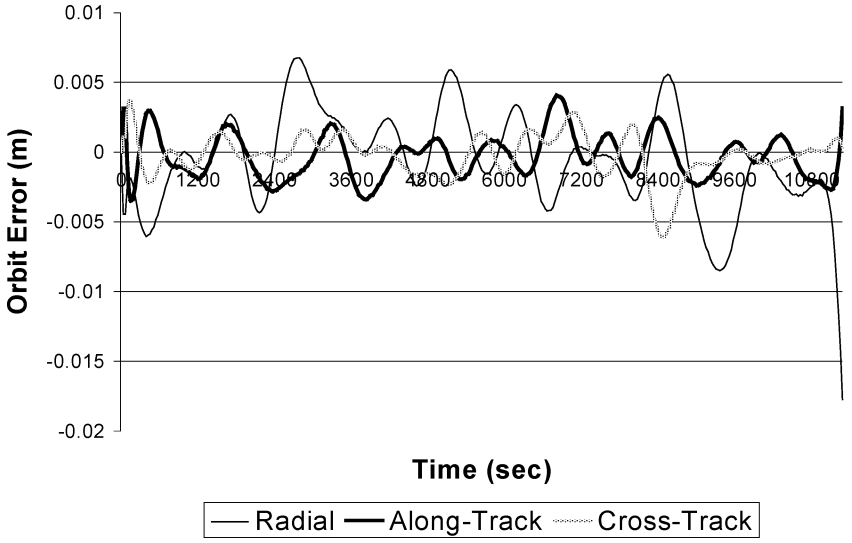

b) Periodic process

Fig. 4 Case 1 RTN orbit errors.

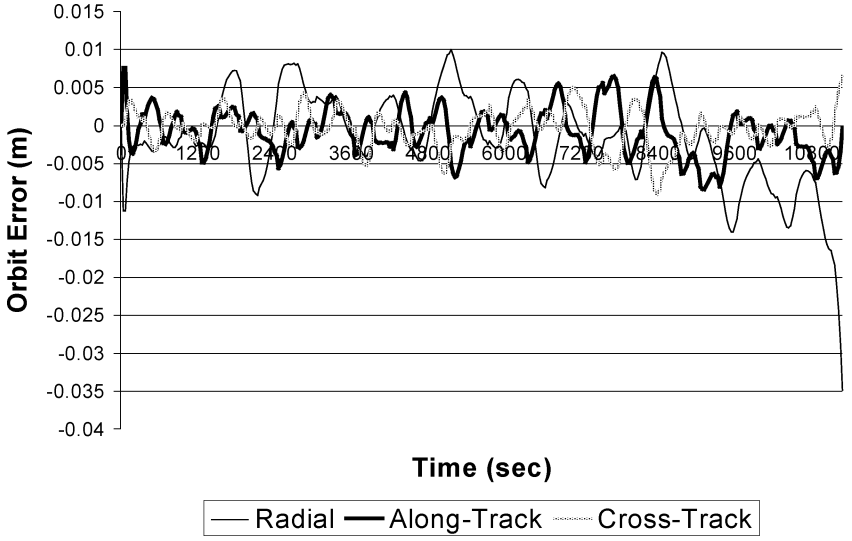

a) GM1 process

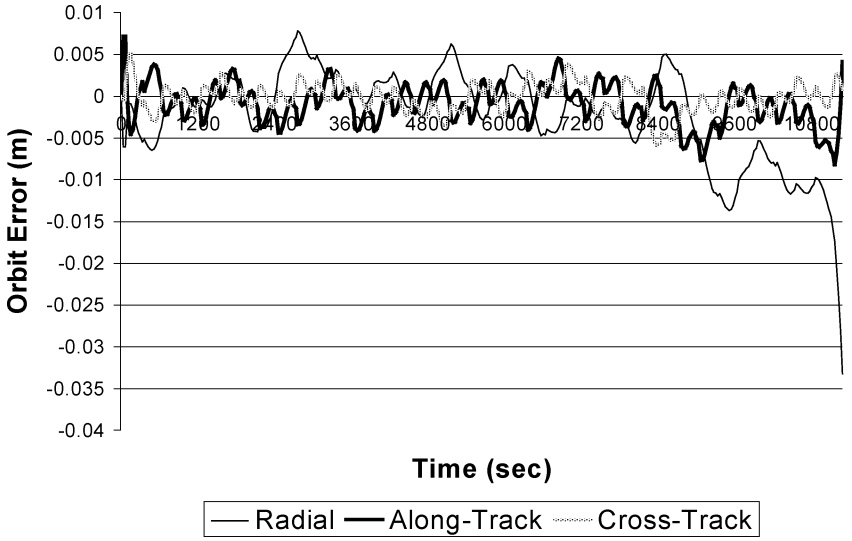

b) Periodic process

Fig. 5 Case 2 RTN orbit errors.

the rms orbit errors were all reduced to the millimeter level. The reason for the centimeter-level orbit errors is that the majority of the remaining errors associated with periodicity did not get absorbed sufficiently with the first-order G–M process. Based on the results described, it can be expected that the accuracy of the orbit would be improved with a random process that can effectively account for periodic behavior of the unknown force.

Figure 6b shows the orbit error obtained with use of the periodic process. Note from Fig. 6b that the majority of smoothed orbit errors is within ± 0.01 m. Compared to those obtained with the first-order G–M process, the improvement of the orbit errors obtained with the periodic process is illustrative of what could be attained after effectively accommodating the periodicity of the unknown force. The periodicities associated with the unknown force, particularly in the along-track direction, remains, indicating that the periodic process did not remove all of the periodic effects of the unknown force. The mean and rms orbit errors are summarized in the rightmost columns of Table 5.

It is clear that a periodic random process is more effective in accommodating the unknown force of periodicity. It is found that, though the unknown forces of cases 1 and 2 are not periodic, the orbit solution obtained with the periodic process is equal to or slightly better than those obtained with the first-order G–M process. Note that improvement in performance with the periodic process is obtained at the cost of increasing the order of noise dynamics by one.

Application to CHAMP Mission

In the context of POD, numerical simulation is a convenient tool to test new methodology and conduct preliminary mission analysis. However, the fidelity of the models used in the numerical simulation is always undermined by the inevitable difference between real-world models and filter models and an absence of a filter models for modeling measurement errors. Hence, the ultimate test for POD is obtained by processing real data. The process noise models and the hybrid strategy are applied to CHAMP data processing, and the results are presented in this section.

CHAMP is a German satellite mission for geoscientific research, managed by GeoForschungsZentrum (GFZ) in Potsdam, Germany. Launched on 15 July 2000, the CHAMP spacecraft occupies a 460-km altitude and 87.3-deg inclination orbit. The orbit characteristics were optimized in such a way that the resulting orbit provides global coverage of the Earth, which is important for the accurate determination of the Earth's gravitational and magnetic fields.

The GPS receiver onboard CHAMP is a Blackjack receiver and is capable of tracking up to 12 GPS satellites at a time. It measures the dual-frequency pseudorange and carrier phase at 10-s intervals. CHAMP carries a laser retroreflector, which provides independent precision range information by the SLR technique. Figure 7 shows the physical layout of the CHAMP spacecraft with location of the flight instruments and subsystems.

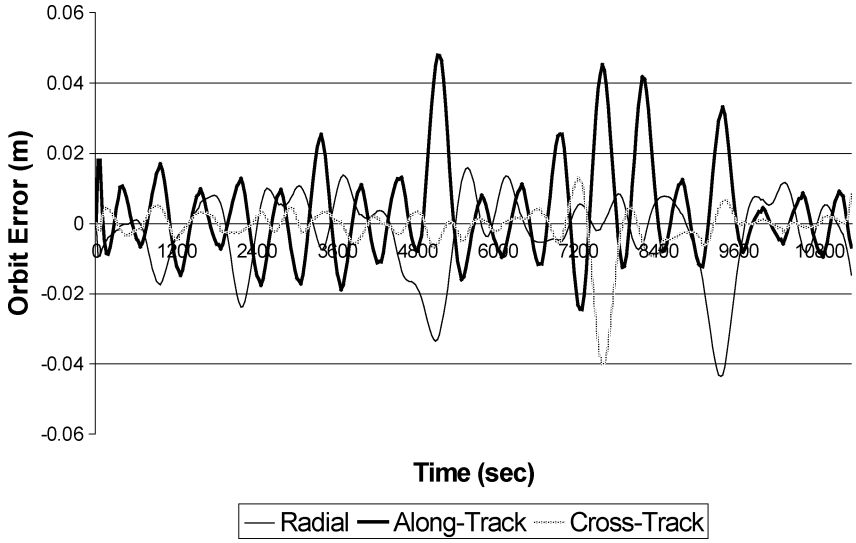

a) GM1 process

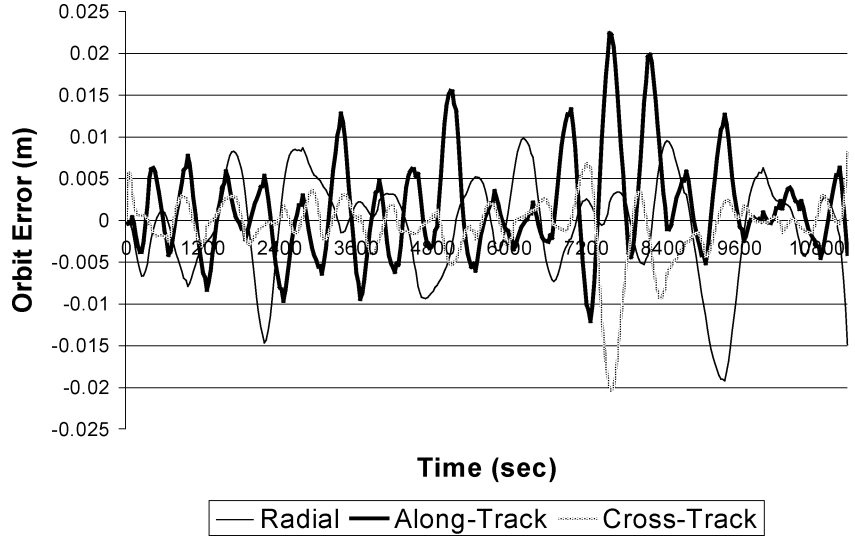

b) Periodic process

Fig. 6 Case 3 RTN orbit errors.

Because the orbit of CHAMP serves as the reference frame for its geodetic measurements, any error in determining the satellite's position will directly affect the quality of the products obtained from the CHAMP measurements. It was, therefore, necessary to compute the CHAMP orbit as accurately as possible, and a goal of this research is to obtain precise orbit solutions of CHAMP by processing GPS L_3 DDHL phase-range measurements and then to assess the relative performance of each process noise model. The L_3 DDHL tracking data of CHAMP were generated with the TEXGAP preprocessing software.[7] With the availability of the broadcast navigation message-containing clock information of the GPS satellites and approximate positions of a user satellite and ground stations, the time tag of the phase-range measurement is corrected against simultaneously observed pseudorange measurement in TEXGAP. Also, outliers are edited out, cycle slips are fixed, and the double-differenced (DD) ambiguity is approximately corrected in this phase.

The CHAMP spacecraft is modeled as a symmetrically perfect and homogeneous sphere or cannonball, with a 521.7-kg mass and an area-to-mass ratio of 0.00138 m^2/kg. The satellite orientation is defined such that the body-fixed $+Z$ axis is always nadir pointing, the $+X$ axis is pointing in the flight direction and aligned with the boom of the spacecraft, and the $+Y$ axis completes a right-handed system.

Note that in GPS-based CHAMP, POD is the GPS orbit constellation and ground network of tracking stations. In this study, the International GPS Service (IGS) orbits were used as observations in a batch orbit fitting. This is because the visibility of each GPS satellite to CHAMP varies rapidly due to the very fast motion of CHAMP. As a result, only a few GPS satellites are available at a specific epoch, and the range information of an individual GPS satellite, throughout the entire data span, can be limited and sparse.

Along with the CHAMP flight receiver, a set of ground receivers is needed to form DDHL measurements, and 35 IGS ground stations were chosen for the study. An elevation angle cutoff of 15 deg was applied to the ground receiver, and a cutoff angle of 0 deg was applied to the CHAMP flight receiver.

After computation of the GV3 hybrid orbit solution, several measures can be used for orbit error verification purposes such as orbit overlap statistics, orbit comparison against other orbit solutions, and SLR residual analysis. Note that to assess the accuracy of an orbit solution through the orbit comparison test, the level of orbit error for the reference orbit needs to be established for the time span of interest. By the use of the SLR tracking data, the radial orbit accuracy can be determined. In this study, CSR CHAMP orbit solutions that were computed from the MSODP software package were chosen to serve as a reference orbit.

MSODP orbit solutions for days 140–144, 2001 (20 May 2001–24 May 2001) were selected for comparison with the GV3 orbits. Five 30-h arcs of CHAMP tracking data that were centered at noon of each day were used to generate the GV3 CHAMP orbit ephemerides,

with 30-s spacing between state elements. This provides a 6-h orbit overlap between two consecutive days. The orbit solutions obtained with each data arc were concatenated to yield single 5-day CHAMP ephemerides. Because the quality of the orbits generally degrades at both boundaries of data arc, the middle 24-h orbit solutions were used to construct the 5-day CHAMP ephemerides.

The reference frame, force, and measurement models used in processing CHAMP data are summarized in Tables 6–8 (Refs. 9–13). The parameters estimated in the solution scenario are summarized in Table 9. In the final sequential filtering/smoothing, the parameters computed dynamically were held fixed, and the state of CHAMP was reestimated sequentially. For process noise parameters, the steady-state uncertainty was chosen by conducting a parameter search with time constant set to 10 min. Solutions were generated for different levels of uncertainties. The value of the steady-state uncertainty was chosen such that the 5-day average of the 6-h radial orbit overlap was minimum. The frequencies of the unknown acceleration were selected by inspection of the estimates of the unknown acceleration.

Table 6 Reference frame models

Model	Reference
Inertial coordinate system	J2000
Precession/nutation, planetary ephemerides	JPL-DE405
Polar motion, UT1-TAI	International Earth Rotation Service (IERS)
Station coordinates, plate motion	ITRF2000
Reference ellipsoid	$a_e = 6{,}378{,}137$ m, $1/f = 298.257$

Table 7 Measurement models

Model	Application
Troposphere	Mapping temperature test
Ionosphere	Dual frequency correction applied
Relativistic correction	Applied
Center of mass offsets	Applied to GPS and CHAMP
Phase wraparound	Applied
Ocean loading	IERS
Geometric tides	Applied
Rotational deformation	Applied

Results

GPS Orbits

It is important to determine the GPS orbits as well as possible because the orbit accuracy of the CHAMP satellite obtained by processing the GPS tracking data will be affected by the quality of the GPS orbits. Figure 8 shows the rms orbit differences of the fit for 29 GPS satellites that were averaged over five days. Note

Table 8 Force models

Model	System
	CHAMP and GPS
GM	398,600.4415 km^3/s^2
Geopotential	TEG4 (Ref. 9) 99×99 for CHAMP, 12×12 for GPS, Zonal rates $\dot{J}_2 = -2.6 \times 10^{-11}$/yr
N-body	JPL DE-405
Solid Earth tides	Wahr's theory
Ocean tides	CSR TOPEX_3.0 (Ref. 10)
Rotational deformation	Applied
Relativity	All geocentric effects
	CHAMP
Solar radiation pressure	$P = 4.56 \times 10^{-6}$ N/m^2 at 1 AU, conical shadow
Earth radiation pressure	Albedo and infrared second-degree zonal model[11]
Atmospheric drag	Drag temperature model[12]
	GPS
Solar radiation pressure	ROCK4 T20, 30 model,[13] conical shadow
Earth radiation pressure	Not applied
Atmospheric drag	Not applied

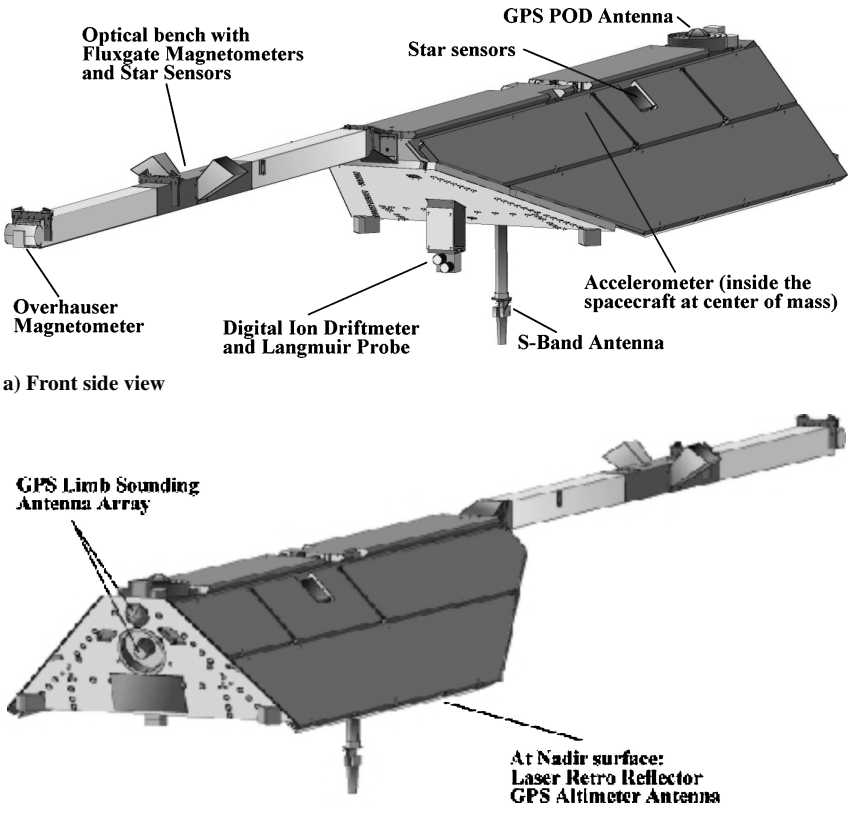

Fig. 7 CHAMP satellite (courtesy GFZ, 2000).

from Fig. 8 that the selected parameterization for GPS orbits yields centimeter-level rms differences in all three components. The highest rms differences were obtained for pseudo-random noise (PRN) 17, and they were about 7.3 cm in the along-track and 5.5 cm in the radial direction. Note from Fig. 8 that most radial rms differences of GPS satellites are at the level of 3.5 cm. For each GPS satellite, the rms difference in along-track direction is the greatest among three components. The hybrid POD strategy for CHAMP was employed after converged GPS orbits were obtained. Note that fixing the GPS orbits prevents them from absorbing part of the CHAMP mismodeled dynamics. This is similar in concept to fixing the location of ground stations when adjusting the state of the CHAMP satellite in the POD process.

MSODP Orbits

Several studies on T/P orbit accuracy show that the orbit comparison test is a conservative measure of orbit errors.[2,14] Before the orbit comparison test is carried out, the important sources of reference frame, force, and measurement model differences between two POD software packages must be identified because differences in the satellite force and measurement models can bias the comparison. Additionally, the estimation scenario employed in generating the orbit solution must be taken into consideration.

Because of their evolution history, the following differences between MSODP and the GV3 software packages were unavoidable. The planetary ephemeris in MSODP was JPL DE-200, whereas JPL DE-405 ephemeris was used in GV3. Station coordinates and velocity used in MSODP were obtained from International Terrestrial Reference Frame (ITRF)1997, whereas GV3 used the station coordinates and velocity from the ITRF2000. It was found, however, that the effect due to these reference frame differences is only at the level of few millimeters. There were also differences in implementation of force models. Although the same TEG4 gravity field[10] is used in both software packages, MSODP additionally employs the technique of postlaunch tuning of the gravity field to remove remaining gravity error, whereas GV3 uses the sequential process noise formulation. MSODP employs a variable cross-sectional model to accommodate the effect of nonconservative forces, whereas GV3 uses a simpler constant cross-sectional model. Such differences can result in a few centimeter orbit differences in along-track and cross-track components, particularly in a high geomagnetic activity environment.

When the measurement models are compared, one difference is the source of meteorological data, which can generate the difference of pass-dependent tropospheric zenith delay. In MSODP, daily values of temperature, atmospheric pressure, and humidity for each station are linearly interpolated from the meteorological measurement data file. In GV3, the nominal values for temperature, atmospheric pressure, and humidity are used for all ground stations. Numbers of observations included in the solutions were different due to differences in elevation angle cutoff for the satellite-to-satellite range. Whereas DDHL data of the CHAMP satellite with elevation angles below 5 deg were edited out in MSODP, GV3 applied a 0-deg elevation angle cutoff.

In addition to the preceding filter model differences, different estimation strategies were employed in the calculation of orbit solutions. Whereas the GPS orbits were directly interpolated to the IGS GPS ephemerides in MSODP, GV3 used the batch orbit fitting method to approximate the same ephemerides. As shown in Fig. 8, one can determine the level of position differences in the GPS orbits. To compute the CHAMP orbits, MSODP employed the fully dynamic approach, coupled with gravity tuning technique. The parameterized batch filter implemented in MSODP adjusts the initial position and velocity of the CHAMP and some dynamic spacecraft parameters, such as atmospheric drag parameters with a subarc length of one revolution and empirical along-track and cross-track accelerations with a subarc length of one-half of a revolution.

To obtain an indication of the accuracy of MSODP orbit solutions, the rms of the DD residuals, the orbit overlap agreement,

Table 9 Estimation scenario

Estimated parameter	Parameterization	A priori constraint
	CHAMP	
Epoch state	Position and velocity	1 km and 0.1 m/s
Drag coefficient	1-h subarc	3.0
Phase center offset	Radial	10 m
Empirical acceleration	1-revolution subarc T, N (1 cycle per revolution)	No a priori
Process noise parameter	$\sigma = 1.0 \times 10^{-9}$ m/s^2, $\varpi = 1.16 \times 10^{-3}$ rad/s	
	GPS	
Epoch state	Position and velocity	1 km and 0.01 m/s
Solar radiation pressure	8-h subarc	3.0
Empirical acceleration	8-h R, N (1 cpr)	No a priori
Tropospheric wet delay	2.5-h subarc	0.5 m
DD ambiguity	Constant over a continuous pass	1.0×10^8

Table 10 RMS of DD residuals of MSODP orbit solution and GV3 hybrid orbit solutions for days 140–144, 2001

Orbit solution	RMS, cm
MSODP	1.14
Case 1	1.32
Case 2	1.09

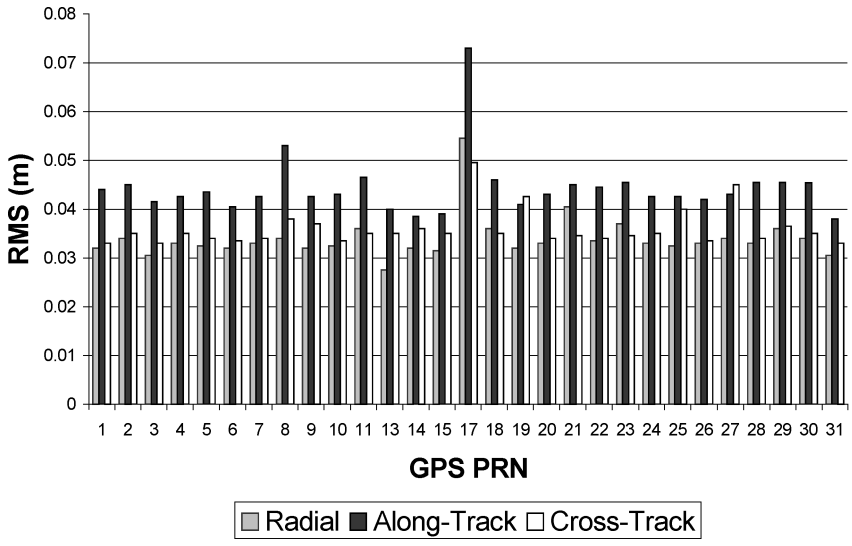

Fig. 8 RTN orbit difference vs GPS satellite PRN.

and SLR analysis results are summarized in Tables 10, 11, and 12, respectively. Individually, quantities such as the orbit overlap and the rms of fit are not sufficient to assess the orbit accuracy. This is because the common correlated errors are eliminated from the orbit overlaps, and the SLR residual fit reflects the accuracy of orbit only for a limited portion of the orbit because of the relatively small number of SLR tracking data. Together, however, these quantities provide a good measure for the orbit accuracy. Thus, the analysis of orbit overlaps and SLR residual rms indicates that the MSODP orbit solutions have a radial orbit accuracy at the level of 3–5 cm on a consistent basis and better than 10 cm in three dimensions. Note that none of SLR measurements was edited out according to elevation angle.

Performance Evaluation and Orbit Quality Assessment

As described, CHAMP data were processed in such a way that a 6-h overlap interval was generated for two adjacent arcs. Although the same data were used in the overlap interval, the orbit solutions of the CHAMP satellite were only partially correlated due to independent orbit determination of GPS satellites. Therefore, the orbit overlap agreement is one indicator of orbit quality and consistency.

Moreover, in the context of hybrid POD, orbit overlap statistics can be used as a performance index in searching for the optimal steady-state uncertainty of process noise, particularly for nonaltimetric satellites. This is simply because there are no altimeter data for external orbit accuracy assessment with CHAMP. Hence, the averaged rms of radial orbit overlap agreement for CHAMP was computed by varying the steady-state uncertainty, and the overall trend is plotted in Fig. 9.

Table 11 Orbit overlap 4 h for days 140–144, 2001

Orbit solution	Bias σ, cm			Three-dimensional RSS
	Radial	Along track	Cross track	
MSODP	0.5 (0.2)	0.9 (0.4)	0.4 (0.1)	1.1
Case 1	2.4 (0.14)	5.2 (1.5)	3.4 (0.6)	6.7
Case 2	2.3 (0.09)	5.1 (1.4)	3.5 (0.7)	6.6

Table 12 Results of SLR residual analysis for days 140–144, 2001[a]

Orbit solution	Number of data	Bias σ	RMS
	SLR residuals		
MSODP	955	−1.47 (0.38)	3.35
	High elevation SLR residuals (>70 deg)		
MSODP	10	−1.64 (1.30)	2.09

[a]Units in centimeters.

Note from Fig. 9 that any level of steady-state uncertainty in the range from 1.0×10^{-9} to 1.0×10^{-11} m/s^2 yields a CHAMP radial overlap of 4 cm or less. Based on the averaged rms radial overlap agreement, a steady-state uncertainty of 1.0×10^{-9} m/s^2 was chosen.

Two hybrid solutions were obtained using different process noise models, similar to the simulation study: The case 1 hybrid solution is obtained with a first-order G–M random process, and the case 2 hybrid is obtained with a periodic random process. Table 11 lists the case 1 hybrid solution for 4-h orbit statistics, together with orbit overlap of case 2 and MSODP orbit solutions. The rms of DD residuals from GV3 hybrid orbits and MSODP are given in Table 10.

The discrepancy in orbit overlap statistics between the GV3 hybrid orbits and the MSODP orbit is probably due to the different treatments of the GPS orbits in both software packages. As described earlier, GV3 used the batch orbit fitting method to compute the GPS orbits, whereas MSODP directly interpolated the IGS ephemerides. In GV3, the independent orbit determination of the GPS orbits was carried out for each data arc, and this results in some orbit differences of the GPS orbits for overlapping intervals, depending on which data arc the GPS orbits belong to. In MSODP, however, the identical GPS orbits are used in calculating the orbit overlap difference, provided that the same interpolating algorithm is used. Hence, the GPS orbits are essentially the same for the overlapping period regardless of the data arc in MSODP. In Fig. 8, the radial orbit differences are at the level of 3.0–3.5 cm, which gives an indication of the radial orbit differences resulting from the batch orbit fitting. Notice that the radial rms fits for hybrid solutions are close to the level of GPS orbit difference mentioned before. Although such orbit differences in GPS ephemerides are generally alleviated through a DD process of the tracking data, they cannot be completely eliminated. The remaining part of the radial orbit differences will affect the CHAMP orbit solution. Hence, it is possible that the orbit overlap statistics for GV3 hybrid solutions can be improved by application of a direct interpolation method to GPS ephemerides. When hybrid solutions are compared with each other, the hybrid orbit obtained with periodic random process shows more consistency in the radial and along-track components than those obtained with the first-order G–M process. In cross track, case 1 provides a better orbit overlap agreement than case 2.

Next, two hybrid solutions were compared with MSODP orbit solutions. Figure 10 shows the position differences between the MSODP orbit solution and the hybrid orbit solution obtained with the first-order G–M random process (case 1). The position differences between the MSODP orbit solution and the hybrid orbit solution obtained with periodic random process (case 2) is shown in Fig. 11. Note that the orbit differences are generally within ±20 cm in both cases and their signatures appear similar to each other.

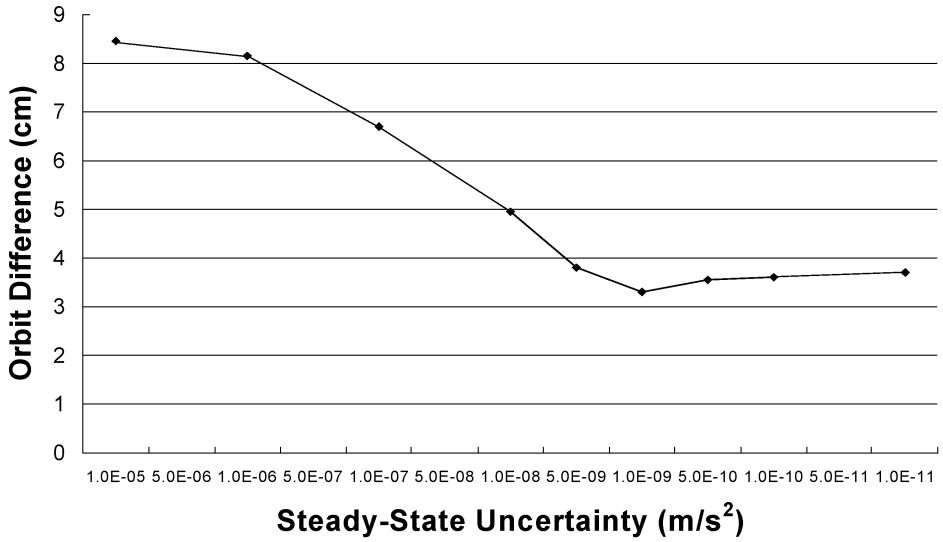

Fig. 9 CHAMP rms radial orbit overlaps vs process noise: ◆, radial.

After a statistical comparison of Fig. 11 to Fig. 10, the mean and rms of orbit differences corresponding to Figs. 10 and 11 are listed in Table 13. Note in Table 13, that the orbit obtained in case 2 yields (in a three-dimensional rss sense) a better agreement with MSODP orbit solution than that obtained in case 1.

Given that the MSODP orbit solution has a radial orbit accuracy of better than 6 cm, the preceding results suggest that the hybrid orbit with periodic random process is more accurate than its G–M counterpart, in an rms sense. Together with orbit overlap statistics, they provide added evidence that a periodic random process can be more effective than the first-order G–M process for the hybrid POD strategy.

Finally, the SLR residual analysis was performed for two hybrid solutions. The results are summarized in Table 14. MSODP was used to generate the SLR residual fit by computation of the difference between SLR range measurements and computed ranges based on the GV3 orbits. Note in Table 14 that SLR residuals are categorized into two groups: SLR residuals and high-elevation SLR residuals. Whereas plain SLR residuals are representative of the absolute orbit position accuracy with radial, along-track, and cross-track components combined, SLR residuals with high-elevation angles (greater than 70 deg) reflect mainly the radial orbit accuracy. Note from Table 14 that the case 2 hybrid orbit yields a better fit than the case 1 hybrid orbit, based on both categories of residuals. Note that the radial orbit accuracy of case 2 is better than case 1. This is partly because the radial orbit overlap agreement is used as a performance

Table 13 Orbit differences between GV3 hybrid orbit solutions and MSODP orbit solutions for days 140–144, 2001

	Radial		Along track		Cross track		Three-dimensional
Case	Mean	RMS	Mean	RMS	Mean	RMS	RSS
1	1.19[a]	6.14	−3.36	12.03	−1.84	9.86	16.72
2	1.17	5.87	−3.22	11.42	−1.88	9.96	16.24

[a]Units in centimeters.

Table 14 Results of SLR residual analysis for GV3 hybrid orbit solutions for days 140–144, 2001

	SLR residuals			High elevation SLR residuals (>70 deg)		
Case	Number of data	Bias σ[a]	RMS[a]	Number of data	Bias σ[a]	RMS[a]
1	955	−0.57 (1.65)	13.34	10	0.66 (4.80)	4.90
2	955	0.01 (1.89)	12.96	10	2.30 (1.16)	2.72

[a]Units in centimeters.

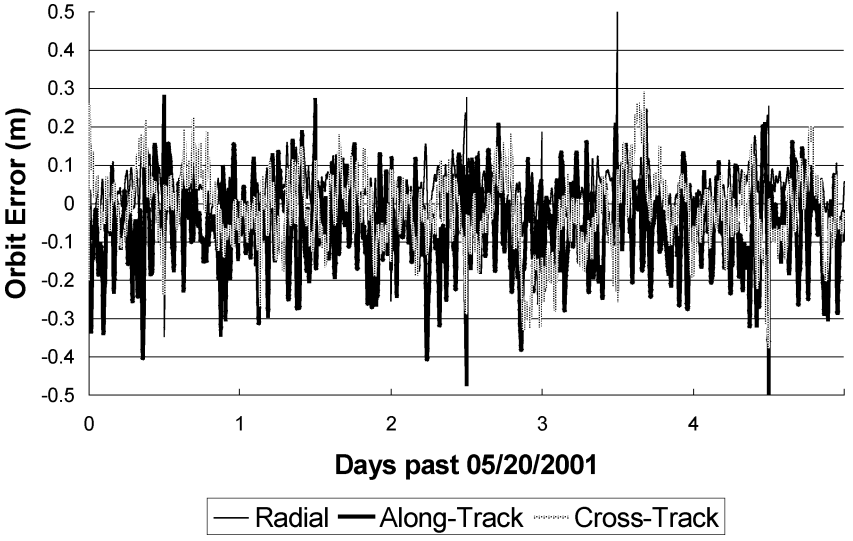

Fig. 10 RTN orbit differences between case 1 orbit with MSODP orbit.

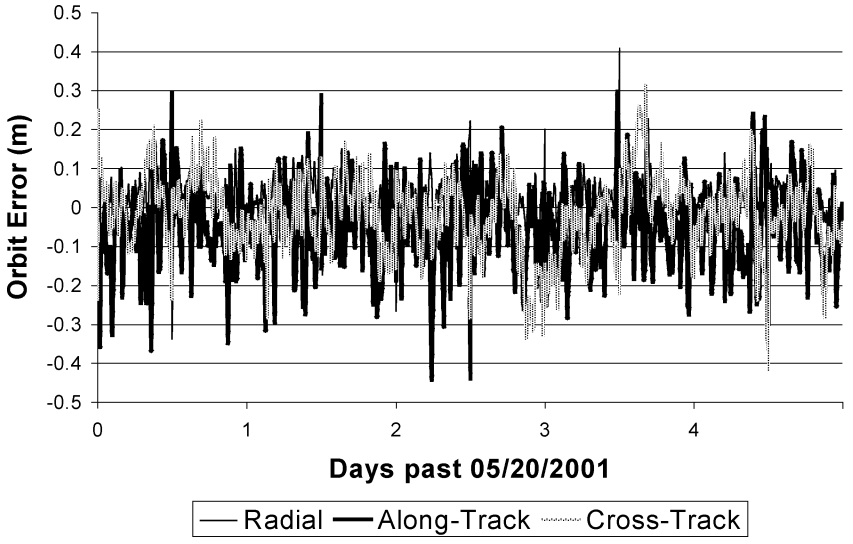

Fig. 11 RTN orbit differences between case 2 orbit with MSODP orbit.

index to search for the optimal steady-state uncertainty of the process noise. It is likely that the orbit errors of the GPS satellites in the along-track component, which is typically the worst among three body-fixed components, contributed to the somewhat large overall rms of plain SLR residuals.

Conclusions

From the numerical simulation, it was concluded that the hybrid POD strategy with a periodic random process could provide an improvement over the first-order G–M process, particularly in accommodating unknown forces that exhibit periodic behavior. The improved performance is mainly because it can be more effective in reducing the part of the orbit error caused by unknown accelerations that are periodic. Additionally, the estimation errors can be further reduced, in general, through the use of a higher-order estimation technique. Whereas the first-order G–M process is, by definition, dependent only on the value at one point immediately in the past, the second-order periodic process is dependent on two consecutive points in the past. Consequently, more accurate prediction and, thereby, improved performance, can be expected.

Evidence (the orbit overlap statistics, the orbit comparison results, and SLR residual analysis) obtained by processing the real tracking data from CHAMP indicate that the hybrid orbit solution with the periodic random process can provide an improvement over that with the first-order G–M random process. Based on orbit comparison criteria (Table 13), the radial orbit accuracy of the GV3 hybrid orbit achieved for the CHAMP satellite with an altitude of 460 km, is within 6 cm RMS. Based on the high elevation SLR residual rms (an absolute measure of orbit accuracy), the radial orbit accuracy is better than 3-cm rms. Finally, it is clear from Table 14 that the hybrid orbit with the periodic random process yielded a better agreement in an rms sense with SLR tracking data than that with the first-order G–M random process. The rms of SLR residuals indicates that the orbit accuracy of the hybrid orbit solution is at the level of less than 3 cm in radial direction and within 13 cm in three dimensional.

Acknowledgment

The first author acknowledges H. J. Rim of the Center for Space Research for his contributions on satellite laser range residual analysis.

References

[1]Fu, L. L., Christensen, E. J., Lefebvre, M., and Menard, Y., "TOPEX/Poseidon Mission Overview," *Journal of Geophysical Research*, Vol. 99, No. C12, 1994, pp. 24,369–24,381.

[2]Schutz, B. E., Tapley, B. D., Abusali, P. A. M., and Rim, H. J., "Dynamic Orbit Determination Using GPS Measurements from TOPEX/POSEIDON," *Geophysical Research Letters*, Vol. 21, No. 19, 1994, pp. 2179–2182.

[3]Yunck, T. P., Bertiger, W. I., Wu, S. C., Bar-Sever, Y., Christensen, E. J., Haines, B. J., Lichten, S. M., Muellerschoen, R. J., Vigue, Y., and Willis, P., "First Assessment of GPS-Based Reduced Dynamic Orbit Determination on TOPEX/POSEIDON," *Geophysical Research Letters*, Vol. 21, No. 7, 1994, pp. 541–544.

[4]Tapley, B. D., Ries, J. C., Davis, G. W., Eanes, R. J., Schutz, B. E., Shum, C. K., Watkins, M. M., Marshall, J. A., Nerem, R. S., Putney, B. H., Klosko, S. M., Luthcke, S. B., Pavlis, D. E., Williamson, R. G., and Zelensky, N. P., "Precision Orbit Determination for TOPEX/Poseidon," *Journal of Geophysical Research*, Vol. 99, No. 12, 1994, pp. 24,383–24,404.

[5]Bertiger, W. I., Bar-Sever, Y. E., Christensen, E. J., Davis, E. S., Guinn, J. R., Haines, B. J., Ibanez-Meier, R. W., Jee, J. R., Lichten, S. M., Melbourne, W. G., Muellerschoen, R. J., Munson, T. N., Vigue, Y., Wu, S. C., Yunck, T. P., Schutz, B. E., Abusali, P. A. M., Rim, H. J., Watkins, M. M., and Willis, P., "GPS Precise Tracking of TOPEX/POSEIDON: Results and Implications," *Journal of Geophysical Research*, Vol. 99, No. C12, 1995, pp. 24,449–24,464.

[6]Bierman, G. J., *Factorization Methods for Discrete Sequential Estimation*, Academic Press, Orlando, FL, 1977, Chaps. 6, 7, and 10.

[7]Rim, H. J., "TOPEX Orbit Determination Using GPS Tracking System," Ph.D. Dissertation, Dept. of Aerospace Engineering and Engineering Mechanics, Univ. of Texas, Austin, TX, Dec. 1992.

[8]Muellerschoen, R. J., Lichten, S. M., Lindquister, U. J., and Bertiger, W. I., "Results of an Automated GPS Tracking System in Support of TOPEX/POSEIDON and GPSMet.," *Proceedings of ION GPS-95*, Inst. of Navigation, 1995, pp. 183–193.

[9]Tapley, B. D., Bettadpur, S., Chambers, D., Cheng, M. K., Choi, K., Gunter, B., Kang, Z., Kim, J., Nagel, P., Ries, J., Rim, H., Roesset, P., and Roundhill, I., "Gravity Field Determination for CHAMP Using GPS Tracking and Accelerometer Data: Initial Results," *EOS Transactions: American Geophysical Union*, 2001 Fall Meeting Supplement, Vol. 82, No. 47, 2001, Abstract G51A-0236.

[10]Eanes, R. J., Schutz, B. E., and Tapley, B. D., "Earth and Ocean Tide Effects on LAGEOS and Starlette," *Proceedings of the 9th International Symposium on Earth Tides*, edited by J. T. Kuo, E. Schweizerbart'sche Verlagsbuchhandlung, Stuttgart, Germany, 1983, pp. 236–249.

[11]Knocke, P. C., "Earth Radiation Pressure Effects on Satellites," Ph.D. Dissertation, Dept. of Aerospace Engineering and Engineering Mechanics, Univ. of Texas, Austin, TX, May 1989.

[12]Barlier, F., Berger, C., Falin, J., Kockarts, G., and Thuillier, G., "Atmospheric Model Based on Satellite Drag Data," *Annales Geophysicae*, Vol. 34, No. 1, 1978, pp. 9–24.

[13]Fligel, H. F., and Gallini, T. E., "Solar Force Modeling of Block IIR Global Positioning System Satellites," *Journal of Spacecraft and Rockets*, Vol. 33, No. 6, 1996, pp. 863–866.

[14]Wu, S. C., Muellerschoen, R. J., Bertiger, W. I., Yunck, T. P., Bar-Sever, Y. E., and Munson, T. N., "Automated Precision Orbit Determination for TOPEX/Poseidon with GPS," *Advances in the Astronautical Sciences*, Vol. 85, 1993, pp. 183–194.

C. McLaughlin
Associate Editor